Discussion on bending-torsion behavior of long wind turbine blades

Gabriel V. P. Lapa[1], Alfredo Gay Neto[1]

[1]*Department of Structural and Geotechnical Engineering, Polytechnic School at University of São Paulo*
380 Professor Luciano Gualberto Avenue, Travessa do Politécnico, 05508-010 São Paulo, Brazil
gabriel.lapa@usp.br, alfredo.gay@usp.br

Abstract. In recent years there has been a tendency to increase the size of wind turbine rotors, particularly when considering offshore applications, leading to more capacity for energy extraction from wind. However, there are many engineering challenges to that. Blades become very long, surpassing lengths of 100 meters, and are usually very flexible, which claims a geometrically nonlinear model for evaluation of their structural behavior. In this context, the present work employs an enhanced structural solver to evaluate the behavior of very flexible wind turbine blades. The blades are modeled as beams. Large displacements and finite rotations are assumed to model the kinematics by employing the geometrically-exact theory. To establish a relationship between generalized internal loads and generalized strains we adopt a linear constitutive model such that one can take results from another software (such as BECAS from DTU), directly. This can handle torsion-bending constitutive coupling for a general position of the beam axis, conveniently. The developed solver was used to study general operational conditions, assuming distinct pitch angles for the blade considering the scenario of the wind turbine. The present work brings discussions on the structural behavior, such as internal loads distributions along the blade spam in numerical simulations. The focus is given to the analysis of bending and torsion moments, discussing their aspects when considering such a long and flexible blade in operational conditions.

Keywords: Aeroelasticity, Numerical simulations, Torsional stiffness

1 Introduction

In the last decade, the size of wind turbines has significantly increased. This is driven by the pursuit of higher altitudes where wind speeds are stronger and turbulence is reduced. This advancement allows for greater energy capture and efficiency. A standout example of modern wind turbine design is the IEA 15MW model [1], characterized by a tower standing 150 meters in height and a rotor diameter of 240 meters. The construction of such large rotors claims the use of composite materials, which impart the necessary flexibility and strength to the blades.

Due to their flexibility, wind turbine blades are particularly susceptible to aeroelastic effects, which arise from the interplay between aerodynamics, elasticity, and dynamics. Aerodynamics examines the forces acting on a body under a given load, influenced solely by wind speed and the geometry of the turbine blades. Dynamics considers the impact of inertial forces, while elasticity focuses on predicting the deformation of an elastic body under a specified load [2].

Aeroelastic modeling can be divided into two main components: aerodynamic and structural models. The primary aerodynamic models include the Vortex Panel Methods [3, 4], high-fidelity Computational Fluid Dynamics (CFD) [5], Actuator-type models [6], and the Blade Element Momentum (BEM) model [7]. The BEM model is widely used due to its simplicity and accuracy. Initially proposed by [8], it offers low computational cost and is easily integrated with beam structural models [9]. Software such as OpenFAST [10] and HAWC2 [11] utilize this model.

The structural modeling of wind turbines can utilize either a 3D Finite Element Model (FEM) [12] or 1D beam models. The 1D beam models can be discretized using 1D FEM. However, it is essential to determine the properties of the transverse sections to construct the constitutive matrix for each element. For dynamic or modal simulations, the mass matrix is also required. One way to obtain these properties is through 2D FEM, where the transverse section is modeled in software like BECAS [13], resulting in the constitutive (stiffness) and mass matrices. These matrices can then be used in structural analysis software such as OpenFAST, HAWC2, and Giraffe [14].

This paper aims to study the blade internal loads along the blade span in numerical dynamic simulations, specifically assessing the influence of torsional deformation. The analyses are conducted using the finite element program GIRAFFE, which employs the geometrically-exact beam model and the Blade Element Momentum (BEM) model. The focus is on a wind turbine operating at rated wind speed, a scenario where peak displacement and internal loads occur at the blade root [15].

2 Rotor model

2.1 Geometrically-exact beam model

This document does not aim to exhaustively detail the geometrically-exact beam theory. For an in-depth understanding, refer to [16], [17], and [18]. Instead, the following sections will provide a general overview of the constitutive matrix.

The theory of geometrically-exact beams, introduced by [19], has proven effective in modeling the kinematics of various structures, including thin-walled beams [20], risers [14], and wind turbines [21], [22], [12] and [15]. For wind turbines, comparisons between beam and shell models in scenarios with significant geometric nonlinearity have shown that beam theory accurately captures the overall structural behavior [12], even under large torsional loads [15]. An important aspect of this theory is its ability to handle large displacements, which is very useful in the numerical simulation of the wind turbine rotor.

By considering a homogeneous material and applying generalized Hooke's law, the theory allows for the formulation of a set of constitutive equations suitable for small deformation contexts. These equations can subsequently be integrated into models that account for large rigid body motions, following the principles outlined by [23]. Consequently, the stresses are expressed as:

$$\boldsymbol{\sigma} = \begin{bmatrix} \sigma_{13} \\ \sigma_{23} \\ \sigma_{33} \end{bmatrix} = \begin{bmatrix} G\gamma_{13} \\ G\gamma_{23} \\ E\varepsilon_{33} \end{bmatrix} , \tag{1}$$

where G and E are the shear modulus and Young's modulus, respectively, γ is the shear strain in its respective direction, and ε is the longitudinal strain in the beam axis direction. Thus, relating stress to strain:

$$\boldsymbol{\sigma}^{i+1^r} = \mathbf{D}\boldsymbol{\epsilon}^{i+1^r} , \tag{2}$$

where the superscript "$...^{i+1^r}$" represents the back-rotation operation, excluding the rigid body motion effect. The symbol $\boldsymbol{\epsilon}$ stands for the generalized strain vector, and $\mathbf{D}$ is a tensor derived from integrating the cross-sectional stresses of the beam. In a simple case, it can be defined as:

$$\mathbf{D} = \begin{bmatrix} GA & 0 & 0 & 0 & 0 & 0 \\ 0 & GA & 0 & 0 & 0 & 0 \\ 0 & 0 & EA & ES_1 & ES_2 & 0 \\ 0 & 0 & ES_1 & EI_1 & EI_{12} & 0 \\ 0 & 0 & ES_2 & EI_{12} & EI_2 & 0 \\ 0 & 0 & 0 & 0 & 0 & GJ \end{bmatrix} , \tag{3}$$

where the coefficients GA, EA, ES_1, ES_2, EI_1, EI_2, EI_{12} and GJ stand for properties dependent on the material, the cross-section of the beam, and on the choice of cross-section alignment.

However, wind turbine blades are made of composite materials, and the simplified example provided may not accurately represent their behavior. To better capture the complex behavior, the matrix $\mathbf{D}$ should be fully populated, allowing for the capture of couplings between degrees of freedom. This capability has been implemented in the Giraffe software, thus using a third-party generated matrix $\mathbf{D}$ into the geometrically-exact formulation.

2.2 Rotor modeling

The rotor parameters were extracted from [1] using the latest available version, v1.1. Further details regarding the modeling approach can be found in [24] and [15]. Below is a concise summary.

A preprocessor was developed to convert the IEA 15MW OpenFAST data into GIRAFFE inputs. The blade's prebend, precone, and tilt angles were incorporated as part of the complex geometry. Figure 1 illustrates the rotor of the IEA 15MW turbine, created using GIRAFFE software and visualized with ParaView [25]. The model was adjusted to simulate only the turbine rotor without employing any controller.

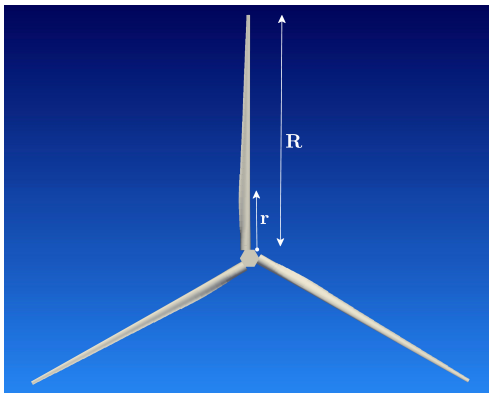

Figure 1. IEA 15MW reference turbine rotor illustration produced by GIRAFFE software and visualized by Paraview. Source: Adapted from [15].

The blade of the IEA 15MW project has 26 cross-sections, including both ends. In GIRAFFE, each element features constant constitutive and sectional mass matrices. The blade models were created using multiples of 25 elements, as shown in Figure 2, which depicts a blade with 25 elements (Figure 2a) and one with 50 elements (Figure 2b). To define these matrices for each element, a linear interpolation was performed along the blade span using IEA 15MW data, considering all elements of the constitutive matrix from eq. 3.

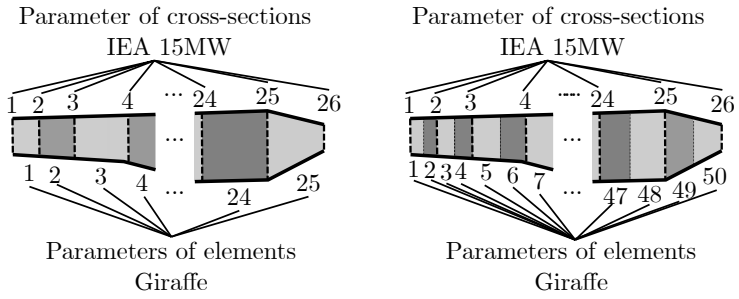

Figure 2. Schematic representation of the elements used in the GIRAFFE modeling along the length of the blade. Source: Adapted from [15].

A mesh analysis was conducted to evaluate different blade meshes (ranging from 25 to 125 elements) to find a balance between computational cost and accuracy. An i7-10750H@2.5GHz computer was used for simulations, each with a duration of 100 seconds. For 25 elements, the simulation took 1757 seconds. For 50, 75, 100, and 125 elements, the simulation times relative to the 25-element case were 2.10, 2.69, 3.91, and 5.08, respectively. Figure 3 shows the flapwise displacement at the blade tip as a function of the number of elements. The displacement remained constant from 50 elements onward. Therefore, a 50-element mesh was selected. The hub was modeled as a rigid body.

As stated in [1], the structural damping for the first modes in the flapwise and edgewise directions was set at 3%. GIRAFFE uses Rayleigh damping, which relates the viscous damping matrix to the mass and stiffness matrices. The natural frequencies for the first vibration modes in the flapwise and edgewise directions are 0.506 Hz and 0.693 Hz [15], respectively, and these frequencies were used to calculate the damping coefficient.

Each element in the GIRAFFE model is set with predetermined aerodynamic parameters. Therefore, aerody-

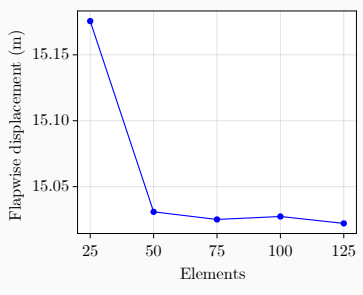

Figure 3. Values of flapwise displacements at the blade tip relative to the number of elements in each blade. Source: Adapted from [24].

namic coefficients for each element were derived based on the nearest available profile, and the chord length and aerodynamic center for each profile were determined through linear interpolation.

Each element in the GIRAFFE model is assigned predetermined aerodynamic parameters. To accurately represent these parameters, the midpoint of each element was used as a reference for positioning it along the blade length. However, it's important to note that these midpoints may not always align precisely with the specified aerodynamic profiles in [1]. Therefore, the aerodynamic coefficients for each element were derived based on the nearest available profile, and the chord length and aerodynamic center for each profile were determined through linear interpolation.

Simulations used a constant wind speed assumption, which varies with height according to a power law [26] with a 0.12 exponent relative to hub speed. The aerodynamic steady-state model was consistently applied and validated against OpenFAST simulations using the Beddoes-Leishman unsteady model, revealing negligible differences [15].

The orientations of the axes are depicted in the local reference frame shown in Figure 4. The Y-axis aligns with the chord line, pointing towards the trailing edge. The X-axis lies in the plane of the cross-section and corresponds to the flapwise direction when the chord line is parallel to the rotor plane. The Z-axis is the longitudinal axis pointing towards the blade tip. The reference point for these axes is located at the pitch axis.

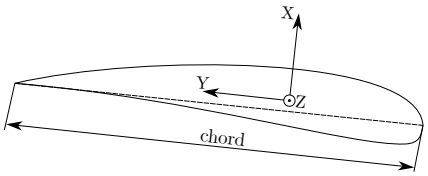

Figure 4. Axis orientation.

3 Simulations and results

This study evaluated the internal forces along the blade under critical conditions occurring at a wind speed of 10.87 m/s [15]. Two simulations were conducted under the same environmental conditions and modeling parameters, differing only in blade torsional stiffness. To determine the appropriate factor for multiplying the torsional stiffness, an analysis was conducted using the values 2, 5, 10, 25, 50, and 100. The results indicate a convergence trend at 100 [24]. The original stiffness was labeled TSx1, while the stiffness amplified by 100 times was labeled TSx100.

The dynamic simulations lasted for 500 seconds, excluding the transient period. Figure 5 illustrates the internal forces along the blade for both the TSx1 and TSx100 cases. The lines represent the mean values, and the shaded regions indicate the maximum and minimum values observed over time (as a time-varying quantity).

It is evident from the results that the torsional effect does not play a significant role in influencing the internal forces along the Y- and Z-axes of the wind turbine blade. The Z-axis, in particular, is predominantly governed by gravitational forces. When the blade is positioned downward, gravity induces traction, leading to maximum force values. Conversely, when the blade is oriented upward, gravity induces compression, resulting in minimum force values along this axis. This gravitational influence underscores the limited impact of torsional stiffness on

the Z-axis forces.

Similarly, the Y-axis experiences oscillations that are primarily driven by the asymmetrical bending of the blade. This bending is a direct consequence of the blade's weight, which causes uneven distribution of forces across its structure. Despite the potential for torsional stiffness to alter the blade's behavior, its effect on the Y-axis forces remains minimal. These findings suggest that while torsional stiffness can affect certain aspects of the blade's performance, its influence on the Y- and Z-axes is overshadowed by other dominant factors such as gravity and the inherent weight distribution of the blade itself.

The X-axis emerges as the most significantly affected by variations in torsional stiffness. This pronounced impact is primarily due to the X-axis's role in influencing the angle of attack, a key factor in the aerodynamic performance of the blade. Torsional stiffness can alter the blade's twist, thereby affecting the angle at which the wind interacts with the blade. As a result, even small changes in torsional stiffness can lead to notable differences in the aerodynamic forces acting along the X-axis.

When analyzing the results at the root of the blade—a critical point of stress concentration—the impact of increased torsional stiffness becomes evident. In the TSx100 case, the mean internal force along the X-axis shows a significant 10.9% increase compared to the TSx1 scenario with the original stiffness. This significant increase in internal force highlights the critical role that torsional stiffness plays in the overall structural integrity of the blade, particularly along the X-axis, which has the smallest second moment of area. Additionally, the TSx100 case exhibits more conservative results.

Figure 6 illustrates the moments along the blade. As in the previous plot, the lines represent the mean values, and the shaded regions indicate the maximum and minimum values observed. The moment component along the X-axis reflects the force along the Y-axis, and vice versa for the Y-axis. As a result, the Y-axis moment component is most influenced by the torsion of the blade. When analyzing the outcomes at the base of the blade, the average internal moment along the Y-axis exhibits a 15.6% rise in the TSx100 scenario relative to TSx1. The torsional moment (Z-axis moment) is two orders of magnitude lower than the moments in the other two directions.

4 Conclusions

The present work brings discussions on the structural behavior, such as internal loads distributions along the blade spam, in numerical simulations. The IEA 15MW wind turbine blade show that it is important to consider the torsion effect in the simulation, mainly the wind direction where the second moment of area is smallest. When considering the amplified torsional stiffness, the results generally tend to be more conservative due to the influence of the angle of attack. Thus, the results from the amplified torsion case can also be applied for sizing purposes.

Acknowledgements. Author Alfredo Gay Neto acknowledges the National Council for Scientific and Technological Development (CNPq), Brazil for the research grant 304321/2021-4 and FAPESP, Brazil for the research grant 2020/13362-1 .

Authorship statement. The authors hereby confirm that they are the sole liable persons responsible for the authorship of this work, and that all material that has been herein included as part of the present paper is either the property (and authorship) of the authors, or has the permission of the owners to be included here.

References

[1] E. Gaertner, J. Rinker, L. Sethuraman, F. Zahle, B. Anderson, G. Barter, N. Abbas, F. Meng, P. Bortolotti, W. Skrzypinski, G. Scott, R. Feil, H. Bredmose, K. Dykes, M. Sheilds, C. Allen, and A. Viselli. Definition of the IEA 15-megawatt offshore reference wind turbine. Technical report, International Energy Agency, 2020.

[2] D. H. Hodges and G. A. Pierce. *Introduction to Structural Dynamics and Aeroelasticity*. Cambridge Aerospace Series. Cambridge University Press, 2 edition, 2011.

[3] K. M. Schweigler. Aerodynamic analysis of the nrel 5-mw wind turbine using vortex panel method, 2012.

[4] A. F. P. Ribeiro, D. Casalino, and C. S. Ferreira. Nonlinear inviscid aerodynamics of a wind turbine rotor in surge, sway, and yaw motions using a free-wake panel method. *Wind Energy Science*, vol. 8, n. 4, pp. 661–675, 2023.

[5] W. Zhang, J. Calderon-Sanchez, D. Duque, and A. Souto-Iglesias. Computational fluid dynamics (cfd) applications in floating offshore wind turbine (fowt) dynamics: A review. *Applied Ocean Research*, vol. 150, pp. 104075, 2024.

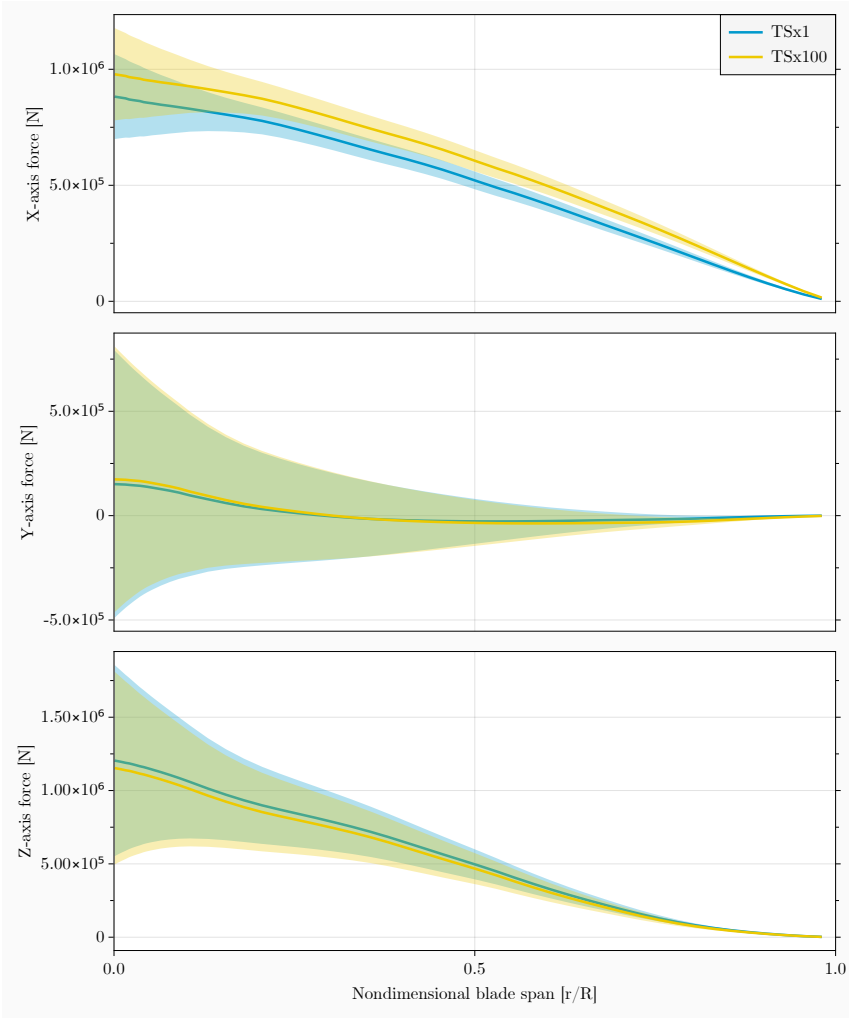

Figure 5. Internal force components across the blade span.

[6] A. ArabGolarcheh, M. Anbarsooz, and E. Benini. An actuator line method for performance prediction of hawts at urban flow conditions: A case study of rooftop wind turbines. *Energy*, vol. 292, pp. 130268, 2024.
[7] U. Boatto, P. A. Bonnet, F. Avallone, and D. Ragni. Assessment of blade element momentum theory-based engineering models for wind turbine rotors under uniform steady inflow. *Renewable Energy*, vol. 214, pp. 307–317, 2023.
[8] H. Glauert. Airplane propellers. *Aerodynamic Theory*, vol. , pp. 169–360, 1935.
[9] L. Wang, X. Liu, and A. Kolios. State of the art in the aeroelasticity of wind turbine blades: Aeroelastic modelling. *Renewable and Sustainable Energy Reviews*, vol. 64, pp. 195–210, 2016.
[10] J. Jonkman. *The New Modularization Framework for the FAST Wind Turbine CAE Tool*, 2013.
[11] T. J. Larsen and A. M. Hansen. *How 2 HAWC2, the user's manual*. DTU Wind Energy Roskilde, 12.8 edition, 2019.
[12] C. J. Faccio Júnior, A. C. P. Cardozo, V. Monteiro Júnior, and A. Gay Neto. Modeling wind turbine blades by geometrically-exact beam and shell elements: A comparative approach. *Engineering Structures*, vol. 180, pp. 357–378, 2019.
[13] K. Branner, J. Blasques, T. n. F. V. Kim, P. Berring, R. Bitsche, and C. Berggreen. Anisotropic beam model for analysis and design of passive controlled wind turbine blades. Technical report, 2012.
[14] A. Gay Neto. Dynamics of offshore risers using a geometrically-exact beam model with hydrodynamic loads and contact with the seabed. *Engineering Structures*, vol. 125, pp. 438–454, 2016.
[15] G. V. P. Lapa, A. Gay Neto, and G. R. Franzini. Effects of blade torsion on iea 15mw turbine rotor operation. *Renewable Energy*, vol. 219, pp. 119546, 2023a.
[16] T. Yojo. *Análise não-linear geometricamente exata de pórticos espaciais (com aplicação a torres de transmissão de alta tensão)*. PhD thesis, Universidade de São Paulo, 1993.

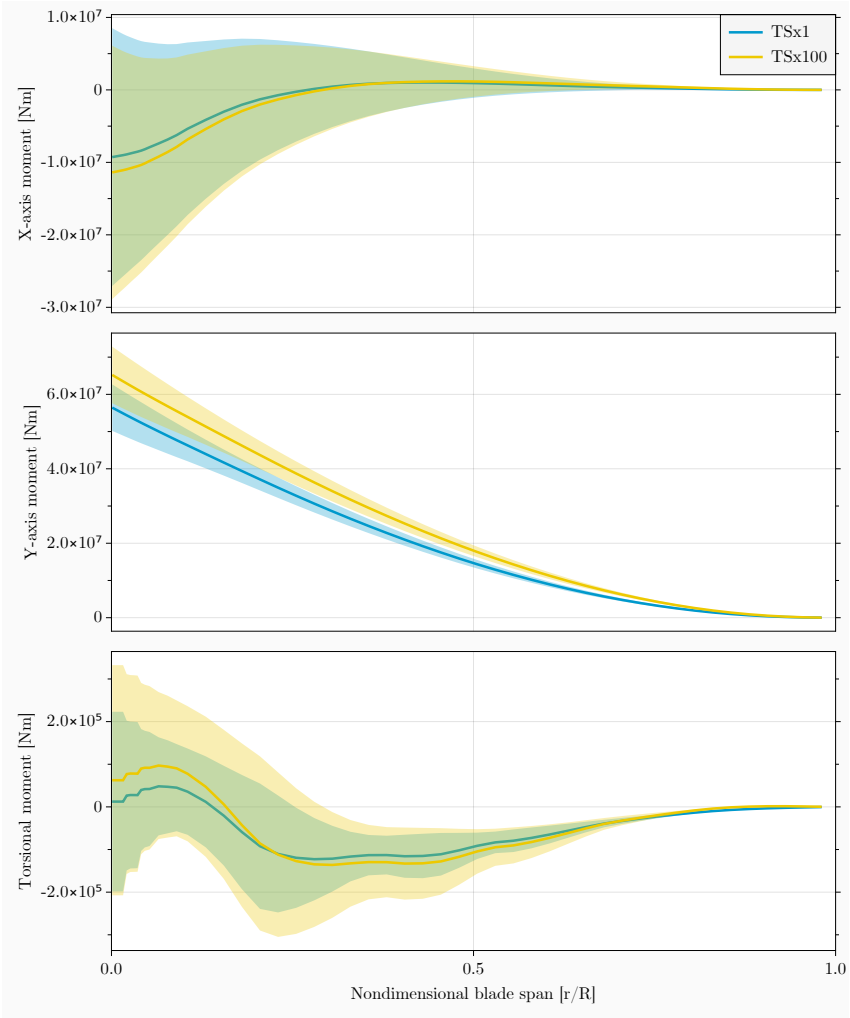

Figure 6. Internal moment components across the blade span.

[17] E. d. M. B. Campello. Análise não-linear de perfis metálicos conformados a frio. Master's thesis, Universidade de São Paulo, 2000.
[18] de M. Lourdes Teixeira Moreira. *Parametrização das rotações em teorias de barras e cascas*. PhD thesis, Universidade de São Paulo, 2009.
[19] J. Simo. A finite strain beam formulation. the three-dimensional dynamic problem. part i. *Computer Methods in Applied Mechanics and Engineering*, vol. 49, n. 1, pp. 55–70, 1985.
[20] E. M. Campello and L. B. Lago. Effect of higher order constitutive terms on the elastic buckling of thin-walled rods. *Thin-Walled Structures*, vol. 77, pp. 8–16, 2014.
[21] L. Wang, X. Liu, N. Renevier, M. Stables, and G. M. Hall. Nonlinear aeroelastic modelling for wind turbine blades based on blade element momentum theory and geometrically exact beam theory. *Energy*, vol. 76, pp. 487–501, 2014.
[22] S. Tang, B. Sweetman, and J. Gao. Nonlinear effects and dynamic coupling of floating offshore wind turbines using geometrically-exact blades and momentum-based methods. *Ocean Engineering*, vol. 229, pp. 108866, 2021.
[23] J. Simo and L. Vu-Quoc. A geometrically-exact rod model incorporating shear and torsion-warping deformation. *International Journal of Solids and Structures*, vol. 27, n. 3, pp. 371–393, 1991.
[24] G. V. P. Lapa, A. G. Neto, and G. R. Franzini. Contribuições ao estudo de aeroelasticidade de pás de turbinas eólicas utilizando o método dos elementos finitos. Master's thesis, Escola Politécnica da Universidade de São Paulo, 2023b.
[25] J. P. Ahrens, B. Geveci, and C. C. Law. Paraview: An end-user tool for large-data visualization. In *The Visualization Handbook*, 2005.
[26] A. Platt, B. Jonkman, and J. Jonkman. Inflowwind user's guide. Technical report, National Wind Technology Center, 2016.